Mon. Not. R. Astron. Soc. **302,** 437–456 (1999)

Magnetic topology and prominence patterns on AB Doradus

J.-F. Donati,[1⋆] A. Collier Cameron,[2⋆] G. A. J. Hussain[2⋆] and M. Semel[3⋆]
[1]*Laboratoire d'Astrophysique, Observatoire Midi-Pyrénées, F–31400 Toulouse, France*
[2]*School of Physics and Astronomy, Univ. St Andrews, St Andrews, KY16 9SS*
[3]*DASoP, Observatoire de Paris-Meudon, F-92195 Meudon-Cedex, France*

Accepted 1998 August 17. Received 1998 August 17; in original form 1998 March 23

ABSTRACT

We report new Zeeman–Doppler imaging observations of the rapidly rotating young K0 dwarf AB Doradus, obtained with the Anglo-Australian Telescope in 1996 December. From such observations, simultaneous brightness and magnetic images of the stellar photosphere of AB Dor were reconstructed at three different epochs.

The magnetic topology of AB Dor is found to be very complex, with at least 12 different radial field regions of opposite polarities located all around the star. Significant azimuthal field fluxes are also detected in the form of one negative polarity region close to the equator, a series of positive polarity patches at intermediate latitudes and an almost complete ring of negative polarity encircling the rotational pole at high latitudes. In particular, the azimuthal polarities we reconstruct are in very good agreement with those obtained by Donati & Cameron, confirming that this field component is directly related to the dynamo-generated large-scale toroidal magnetic structure. The triple polarity latitudinal pattern observed for this structure in the upper hemisphere of AB Dor indicates that the degree of the underlying large-scale poloidal structure in an axisymmetric spherical harmonics expansion is equal to or greater than five. It also strengthens the idea that the dynamo processes operating in AB Dor feature a non-solar component distributed throughout the convective zone.

From the subtle distortion of successive brightness images, we can also confirm the surface differential rotation first measured on this star by Donati & Cameron in both sense and magnitude, with a pole rotating more slowly than the equator by about one part in 220.

Finally, the rotation periods we measure for four prominences (from the recurrence rate of their spectral signatures in Balmer lines) confirm the presumption that such clouds are anchored at intermediate to high latitudes. The intrinsic variability of these prominences is not associated with any abrupt changes in the photospheric brightness or magnetic distributions, implying that they essentially result from the reorganization of coronal field lines.

Key words: line: profiles – polarization – stars: activity – stars: imaging – stars: magnetic fields – stars: rotation.

1 INTRODUCTION

The rapidly rotating K0 dwarf AB Doradus is known to exhibit all kinds of solar-like magnetic phenomena, featuring for example large surface temperature inhomogeneities (e.g. Cameron & Unruh 1994), a hot extended atmosphere with a several million K corona (e.g. Kürster 1996), as well as massive prominences presumably trapped in closed coronal loops near the Keplerian corotation radius (e.g. Cameron & Robinson 1989a, b). However, no information has been available until recently on the engine that drives all such activity phenomena, i.e. the magnetic structure and the underlying dynamo processes.

In 1995 December, phase-resolved spectropolarimetric (i.e. Zeeman Doppler imaging or ZDI) observations from the Anglo-Australian telescope (AAT) revealed that the magnetic topology of AB Dor is extremely complex, comprising up to twelve different radial field regions of opposite polarities located at intermediate to high latitudes (Donati & Cameron 1997). Several patches of azimuthal field (with positive and negative polarities at intermediate and high latitudes respectively) were also detected and tentatively interpreted as a direct detection of the underlying large-scale toroidal field at photospheric level. Altogether, it suggested that the associated dynamo is probably not purely solar-like (i.e. confined to an overshoot layer at the base of the convective zone), but must also

⋆E-mail: donati@obs-mip.fr (JFD); acc4@st-andrews.ac.uk (ACC); gajh@st-andrews.ac.uk (GAJH); semel@obspm.fr (MS)

include a significant component distributed throughout the whole convective envelope. In addition to these results, Donati & Cameron (1997) were also able, from comparing two brightness images of AB Dor recorded eight rotation cycles apart, to detect and measure the surface differential rotation of this object, and prove that it was very much solar-like both in sense (with the equator rotating faster than the pole) and amplitude (with a time for the pole to lap the equator by one full rotation cycle of about 120 d).

We report in this paper new ZDI observations of AB Dor obtained at the AAT in 1996 December. The aim of this new run was to confirm the various results obtained in 1995 December (and in particular the surface differential rotation and topology of large-scale dynamo field), as well as to try to evidence (through higher quality data) potential spatial correlation between magnetic features at photospheric level and prominences in the corona. After quickly describing the new aspects of the instrumental setup and giving a brief log of the observing run (Section 2), we present the brightness and magnetic images we derived from our new data set (Section 3), compare these new results with the previous ones and discuss the implications for our understanding of how dynamo operates in the convective envelope of AB Dor and how prominences relate to the magnetic topology (Section 4).

2 OBSERVATIONS AND DATA REDUCTION

2.1 Instrumental setup

As in 1995 December, we used the 3.9-m Anglo-Australian telescope atop Siding Spring mountain. The observational setup was very similar to that described in Donati et al. (1997) and Donati & Cameron (1997) and consisted of a polarimeter (mounted at Cassegrain focus), a double-fibre link to the UCL Echelle Spectrograph (UCLES) and a Bowen–Walraven image slicer device. With the 31.6 line mm^{-1} grating and the thinned Tektronix 1024×1024 pixel CCD camera, we were able to obtain close to full spectral coverage from 470 to 710 nm in a single exposure. The only difference with the previous experiment is that the magnification of the attendant slicer optics (see Donati et al. 1997 for details) was reduced from 12 to 9.1 to obtain a slit size of 3.8×0.45 mm^2 at the entrance of the spectrograph (18×1.4 pixel at the detector level). The advantage of such a change is that a dekker was no longer necessary at the entrance of the spectrograph (to prevent order overlap in the red part of the spectrum) and that the associated slit shape asymmetries between both orthogonally polarized beams were greatly reduced. The cost is of course that we end up entering the spectrograph with a faster than nominal f/27 beam. However, UCLES optics being vastly oversized, the associated light loss is found to be smaller than when using the dekker. Another advantage of this new setup is that the spectral resolution is increased to 65 000 (including the internal spectrograph aberrations), i.e. about 20 per cent higher than last time.

2.2 Optimal extraction

In total, 366 individual 200-s exposures of AB Dor were recorded in this new run, 83 on the first night (December 23), 78 on the third one (December 25), 11 on the fourth one (December 26), 96 on the fifth one (December 27) and 98 on the seventh and last one (December 29). Most data were recorded in good to moderate seeing conditions (i.e. 1.0 to 1.5 arcsec), except on December 26 where we observed through very thick clouds. Bad weather also prevented us from observing at the beginning of the first night, while we lost two hours at the end of the third one owing to a computer failure. Since a sequence of four successive individual exposures (with adequate positions of the quarter-wave plate) are needed to extract a polarisation spectrum (see Donati et al. 1997 for details), we finally end up with 20 Stokes V spectra of AB Dor on the first night, 19 on December 25, 2 on December 26, and 24 for both fifth and seventh nights (see Table 1 for a complete journal of observations). Both Stokes I and V spectra (and associated error bars) were derived from raw FITS images with a dedicated software package (ESPRIT) mostly inspired from optimal extraction principles (see Donati et al. 1997 for details). The typical time resolution between two successive Stokes I and V spectra is about 260 s and 1040 s respectively (i.e. about 0.6 per cent and 2.3 per cent of the rotational period of AB Dor).

Table 1. Journal of observations. The two first columns list the date and object name, while columns 3, 4 and 6 indicate the Julian date, Universal Time and fractional rotation cycle (in the particular case of AB Dor, using Innis et al.'s 1988 ephemeris), for the first and last subexposure of each continuous series. Column 5 mentions the total number of individual subexposures and polarization sequences in the associated series of subexposures.

Date	Object	JD (2,450,000+)	UT (h:m:s)	n_{exp}	Cycle (11,900+)
1996 Dec. 23	AB Dor	440.9750/440.9911	11:24:01/11:47:11	6/1	35.7408/35.7721
		441.0198/441.1560	12:28:29/15:44:38	45/11	35.8278/36.0924
	Gl 176.3	441.1599	15:50:14		
	AB Dor	441.1639/441.2095	15:56:01/17:01:44	16/4	36.1077/36.1963
	Gl 367	441.2146	17:09:01		
	AB Dor	441.2194/441.2650	17:15:55/18:21:32	16/4	36.2155/36.3041
1996 Dec. 25	AB Dor	442.9108/443.0657	09:51:32/13:34:39	52/13	39.5012/39.8021
		443.0827/443.1580	13:59:05/15:47:33	26/6	39.8351/39.9814
1996 Dec. 26	AB Dor	444.2042/444.2474	16:54:04/17:56:19	11/2	42.0136/42.0976
1996 Dec. 27	AB Dor	444.9272/445.0458	10:15:07/13:05:54	40/10	43.4181/43.6485
		445.0646/445.0974	13:32:59/14:20:18	12/3	43.6850/43.7487
		445.1164/445.2213	14:47:35/17:18:44	36/9	43.7856/43.9894
		445.2394/445.2607	17:44:45/18:15:24	8/2	44.0246/44.0659
1996 Dec. 29	AB Dor	446.9218/447.0506	10:07:21/13:12:50	44/11	47.2927/47.5429
		447.0683/447.1025	13:38:18/14:27:34	12/3	47.5773/47.6437
		447.1233/447.2055	14:57:29/16:55:54	28/7	47.6841/47.8438
		447.2236/447.2624	17:22:00/18:17:51	14/3	47.8789/47.9543

While one aim of this project is to reconstruct brightness and magnetic field images of the surface of AB Dor, another one consists in tracking temporal evolution of these distributions, caused by latitudinal differential rotation for instance. We therefore tried to keep data sets from different nights as separate as possible. However, a closer look at the actual times and dates at which our observations were collected tells us that only data from December 25 to December 29 show a significant overlap in rotational phase, while spectra recorded in the first night end up sampling a different part of the rotation cycle. As stellar surface imaging requires the densest possible coverage of the rotation cycle for optimal performances, we decided to merge the first and third night data sets (into what we will call data set #1 in the following) to maximize phase coverage at this epoch. Note that the few redundant observations between the first and third night (i.e. all spectra collected on December 23 before JD 245 0441.01 an on December 25 after JD 245 0443.07) were simply discarded. Data collected on December 27 and December 29 were kept separate (forming data set #2 and #3 respectively), while those recorded on December 26 were also discarded given their very low quality. We therefore end up with three independent data sets including respectively 129, 96 and 98 Stokes *I* spectra and 32, 24 and 24 Stokes *V* observations. The first set should first provide a good overview of the whole surface of AB Dor. Along with the two other data sets, it should also help us check that surface distributions reconstructed from different data sets are in good mutual agreement, and quantify the time evolution of both brightness and magnetic distributions during our observing run.

As brightness and magnetic surface images of AB Dor do not get significantly distorted by surface differential rotation and intrinsic variability on a time-scale of 2 d (Donati & Cameron 1997), we do not expect any problems in the analysis to result from merging spectra obtained on the first two observing nights in a single data set. We nevertheless incorporated, for this particular data set, the effect of surface differential rotation in the brightness and magnetic image reconstruction process (see Section 3.2) in an attempt to 'rephase' as well as possible spectra obtained on December 23 with those recorded on December 25.

2.3 Least-squares deconvolution

As in Donati & Cameron (1997), we applied ''least-squares deconvolution'' (LSD) to all our Stokes *I* and *V* spectra. This technique, devised by Donati et al. (1997), is similar to other cross-correlation techniques in the sense that it extracts information from every moderate to strong spectral feature in the recorded wavelength domain. The LSD Stokes *I* or *V* profile we obtain for each spectrum with this method can be roughly described as a weighted average of all profiles involved in this procedure. In particular, its relative noise level is considerably reduced compared to that of each single line of the original spectrum. Moreover, as demonstrated in Donati & Cameron (1997), LSD conserves the shape of a pure rotational profile to a very good accuracy, implying that any deviation observed in LSD profiles from this reference level can be considered as real and, in our particular case, ready to be interpreted in terms of surface brightness/magnetic inhomogeneities. The list of spectral lines available for LSD (and in particular their wavelengths, relative central depths and Landé factors) are obtained from a full LTE synthesis with a K0V model atmosphere taken from Kurucz (1993), selecting only those features whose relative central depth (prior to rotation or macroturbulence broadening) exceeds 0.4. In our particular case, up to 1500 spectral lines can be used simultaneously in the analysis.

The final S/N ratio values we obtain in LSD Stokes *I* and *V*[1] spectra (derived by propagating the original spectra error bars yielded by ESPRIT through LSD) are plotted in Fig. 1 for each observing night, with typical values of 1400 (when normalized to a mean line depth of 0.7 instead of 1 as in Donati & Cameron 1997) and 9000. Given the typical S/N ratio of individual Stokes *I* and *V* spectra (165 and 330 respectively), we infer multiplex gains in S/N of 8.5 and 27 respectively.

The Stokes *I* and Stokes *V* dynamic spectra obtained for each night are presented in Figs 2 and 3 respectively, each of them showing clear rotationally modulated brightness and magnetic spot signatures, in the form of line profile distortions travelling from blue to red. The average peak-to-peak amplitude of the Zeeman signatures is about 0.13 per cent, i.e. about 12 times the rms noise level per 3 km s^{-1} bin. The rotational modulation repeats quite well at first order between different nights, whenever two data sets end up having significant phase overlap.

3 RESULTS

3.1 Image reconstruction software

For brightness imaging, we use the two-component model of Cameron (1992) which aims at reconstructing, for each point of the stellar surface, a quantity f describing the local fraction of the stellar surface occupied by cool spots. This quantity, varying from 0 (no spot) to 1 (maximum spottedness), is referred to as 'spot occupancy' in the following. LSD profiles of the K0V star Gl 176.3 and the M4V object Gl 367 are used as template profiles describing the spectral contribution of the photosphere and spot respectively (see Donati & Cameron 1997 for a display). In this context, an integrated model profile associated to a given stellar image viewed at a given rotational phase can be obtained by shifting in velocity and adding up together the spectral contributions of all image pixels.

For magnetic imaging, the model we use is that of Donati & Brown (1997), which assumes that the intrinsic profile is Gaussian and constant over the stellar surface, and the weak field approximation holds. Although very simple, this model is found to be perfectly adequate for describing LSD Stokes *V* profiles averaged over more than 1500 individual spectral features as demonstrated in Donati & Cameron (1997) and Donati et al. (1997). The quantities we reconstruct are the three components of the magnetic field vector in spherical coordinates (i.e. radial, meridional and azimuthal field), weighted by potential surface inhomogeneities in brightness, local magnetic filling factor and central depth of true intrinsic profile.

The maximum entropy reconstruction code we use is that of Brown et al. (1991), which implements Skilling & Bryan's (1984) algorithm for maximum entropy optimization problems.

3.2 Resulting images

The resulting brightness and magnetic images of AB Dor are shown in Fig. 4 (for data set #1), Fig. 5 (for data set #2) and Fig. 6 (for data set #3). As in Donati & Cameron (1997), we used a stellar inclination of 60° and a $v \sin i$ of 91 km s^{-1}. The optimal radial

[1]In the following text, we define the S/N ratio of Stokes *V* spectra as $1/n$ where n is the relative noise level per digital channel. Being roughly equal to the square root of the total number of photons collected in the corresponding bin, this parameter is thus nothing more than a circular polarization spectrum quality indicator, and gives in particular no information about the accuracy to which a potential Zeeman signature may be detected.

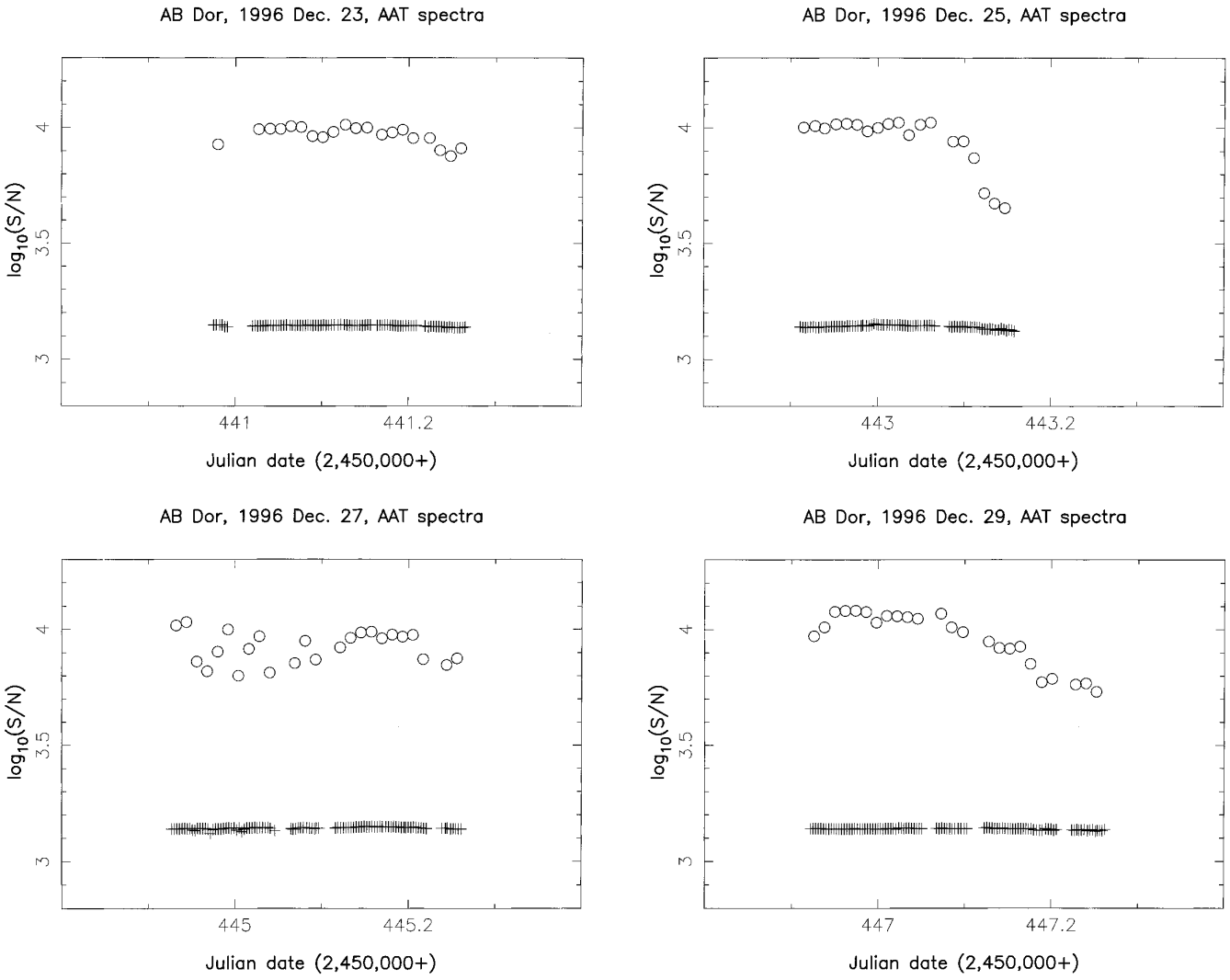

Figure 1. Logarithmic S/N ratio (per 3 km s^{-1} bin) in mean Stokes *I* (plus signs) and *V* (open circles) profiles for both 1996 December 23 (top left), 25 (top right), 27 (bottom left) and 29 (bottom right) observations.

velocity (obtained by minimizing the information content in the derived image as described by Cameron & Unruh 1994) is 30.5 ± 0.5 km s^{-1}, i.e. slightly less but still compatible with the value of 31 ± 1 km s^{-1} found by Donati & Cameron (1997). All images correspond to a unit reduced χ^2 fit to the data. Note that for brightness imaging, LSD template profiles had to be scaled up by about 6 per cent to match the equivalent width of the LSD profiles of AB Dor.

The reconstructed profiles are shown along with the observations in Figs 7 and 8. Given the higher spectral resolution of these new observations (65 000 or 4.6 km s^{-1}), the spatial resolution of these new maps is better, reaching at best 2°.9 in longitude at the stellar equator. Note that a surface differential rotation rate equal to that estimated by Donati & Cameron (1997) was assumed for the inversion of the first data set (for which spectra were collected on a total time span of about 2 d or 4 rotation cycles). The impact of this assumption on the reconstructed images remains however fairly small, consisting essentially in small eastward longitude shifts (of the order of one resolution element at the stellar surface or less) for the brightness/magnetic features observed on December 23 (i.e. located in the [0.8,1.0] and [0.0,0.3] phase intervals).

The code ends up with a total spottedness (defined as the sum over all image pixels of $p_i\, f_i$ where f_i and p_i denote respectively the reconstructed spot occupancy and fractional area of image pixel *i*) of 9.4, 7.6 and 8.1 per cent for data set #1, #2 and #3 respectively. The corresponding mean field strength (defined as the sum over all image pixels of $p_i\, B_i$ where B_i denotes the modulus of the reconstructed field vector at image pixel *i*) are equal to 110, 100 and 100 G. Another way of characterizing the reconstructed distributions is to compute thresholded versions of these images (in which all f_i or B_i pixel values below a given threshold are set to zero), thresholds being set such as the spottedness or mean field strength of the thresholded images are half that of the original images. The 'filling factors' of the original brightness/magnetic distributions are then obtained by summing up the fractional area of all cells in the thresholded image for which f_i or B_i pixel values are non-zero. These filling factors thus represent the fractional stellar surface covered by the darkest/most magnetic regions that enclose 50 per cent of the global spottedness/magnetic field altogether. For our three data sets, brightness/magnetic filling factors are equal to 8 and 15 per cent on average [i.e. comparable to what we find for other late-type rapid rotators, Donati 1999 (Paper II, this issue)], the mean spottedness/field strength within these regions being of the order of 50 per cent and 400 G respectively.

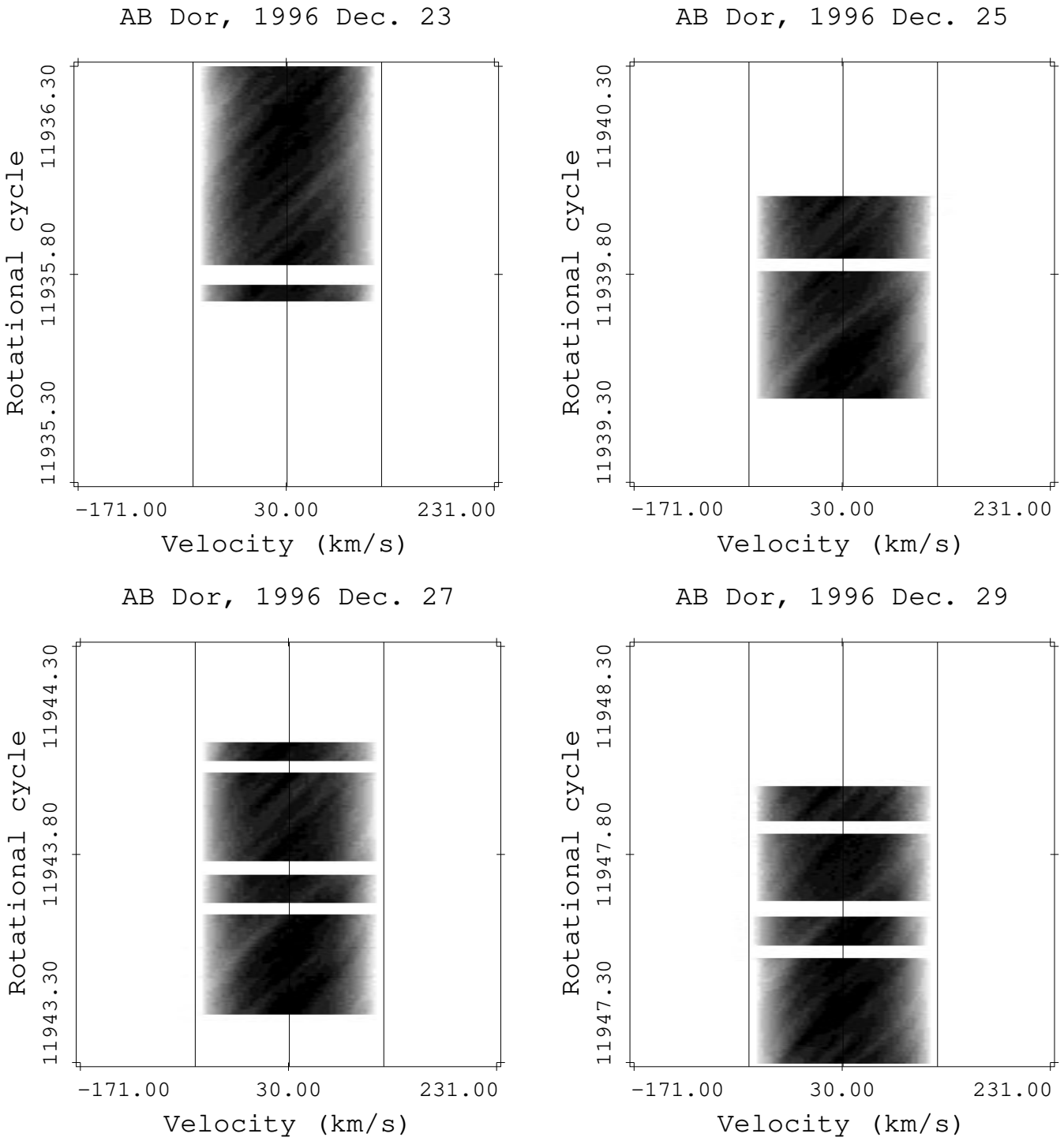

Figure 2. Stokes *I* dynamic spectra of AB Dor in 1996 December 23 (top left), 25 (top right), 27 (bottom left) and 29 (bottom right). The three vertical lines in each plot indicate the rotational broadening (left and right lines) and radial velocity (middle line) of AB Dor. Grey levels code relative intensities (normalized to the continuum level) ranging from 0.965 (black) to 0.993 (white).

At least 10 individual features (at rotational phases 0.00, 0.25, 0.30, 0.35, 0.50, 0.52, 0.68, 0.78, 0.87 and 0.93) gathering in seven main spot groups (at phase 0.00, 0.30, 0.50, 0.68, 0.78, 0.87 and 0.93) can be identified, both in the original Stokes *I* dynamic spectra of Fig. 2 and in the reconstructed brightness maps of Figs 4 to 6 (whenever the corresponding phases are observed). Note in particular that there is a good overall similarity between the different reconstructed distributions, especially in the overlapping phase range (0.50 to 0.95) for which all three maps feature the following.

(i) A Y-shaped spot centred at phase 0.68, including two high-contrast components at intermediate latitudes (25° and 40°) as well as two other weaker ones (at phase 0.60 and 0.75) located at higher latitudes (about 55°).

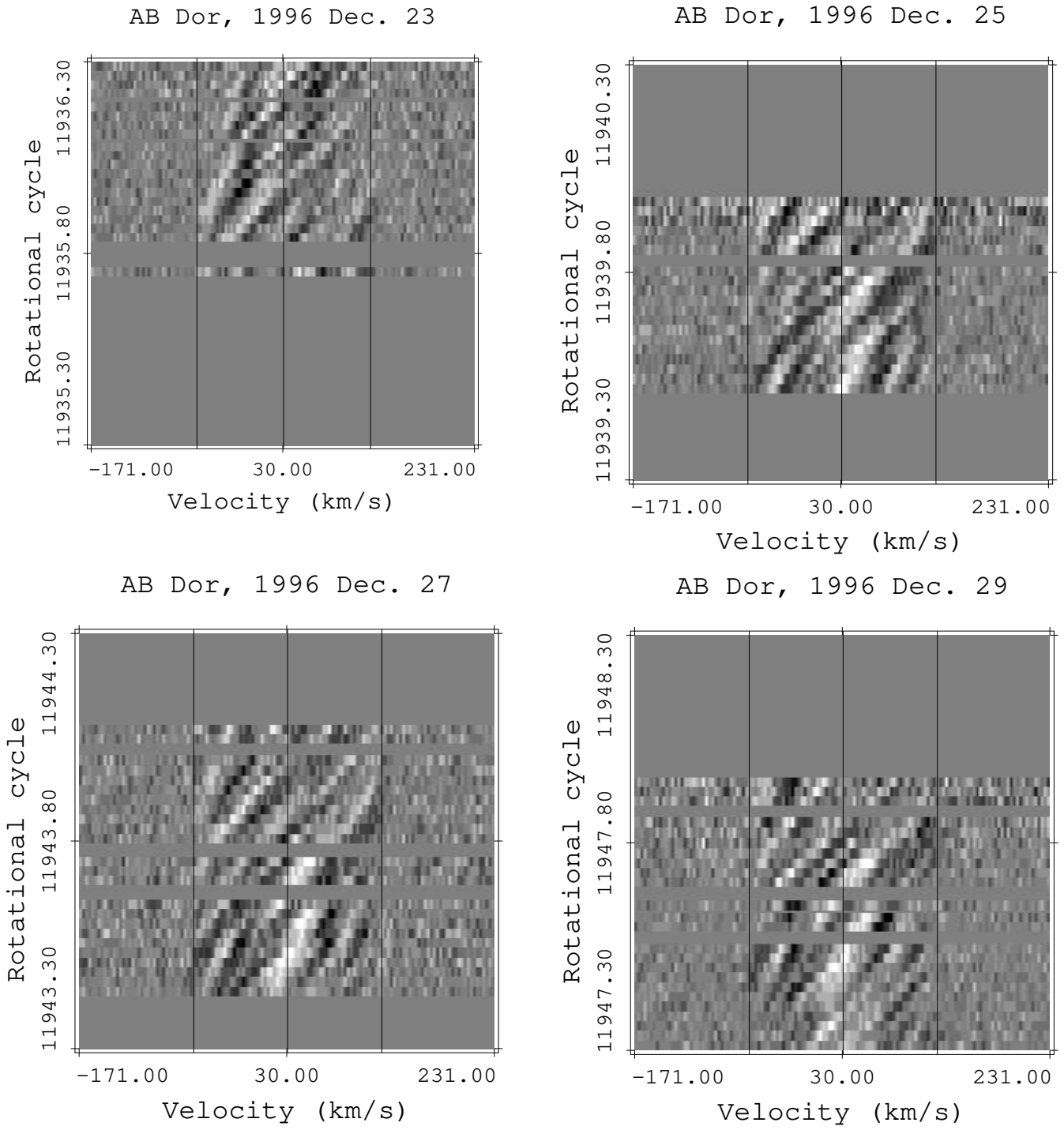

Figure 3. Same as Fig. 2 for Stokes *V* dynamic spectra. Grey levels code relative circular polarization levels (in units of the unpolarised continuum level) ranging from −0.06 (black) to 0.06 per cent (white).

(ii) A triple spot structure around phase 0.93 with two subcomponents at latitude 20° (shifted by about 4 per cent in rotational phase) and a third one at latitude 50°.

(iii) A single feature located at phase 0.87 and latitude 40°.

Some subtle differences can nevertheless be observed between these images (and between the associated data sets as well) even in the overlapping phase range. Apart from the global eastward drift of most equatorial features (caused by surface differential rotation, see Section 4.1 and Donati & Cameron 1997), one can even detect intrinsic variability of surface features. The brightness feature obviously present at phase 0.78 in image #1 has for instance considerably weakened by December 27 and almost completely vanished by December 29. On the opposite, the apparent variability the three other spot groups (at phase 0.00, 0.30 and 0.50) seem subject to is most likely due to the poor coverage obtained at the corresponding phase in at least one of our three data sets. All three images show a clear polar spot (consistent with the permanently flat-bottom Stokes *I* profiles, see Fig. 7), just as most AB Dor images obtained to date do.

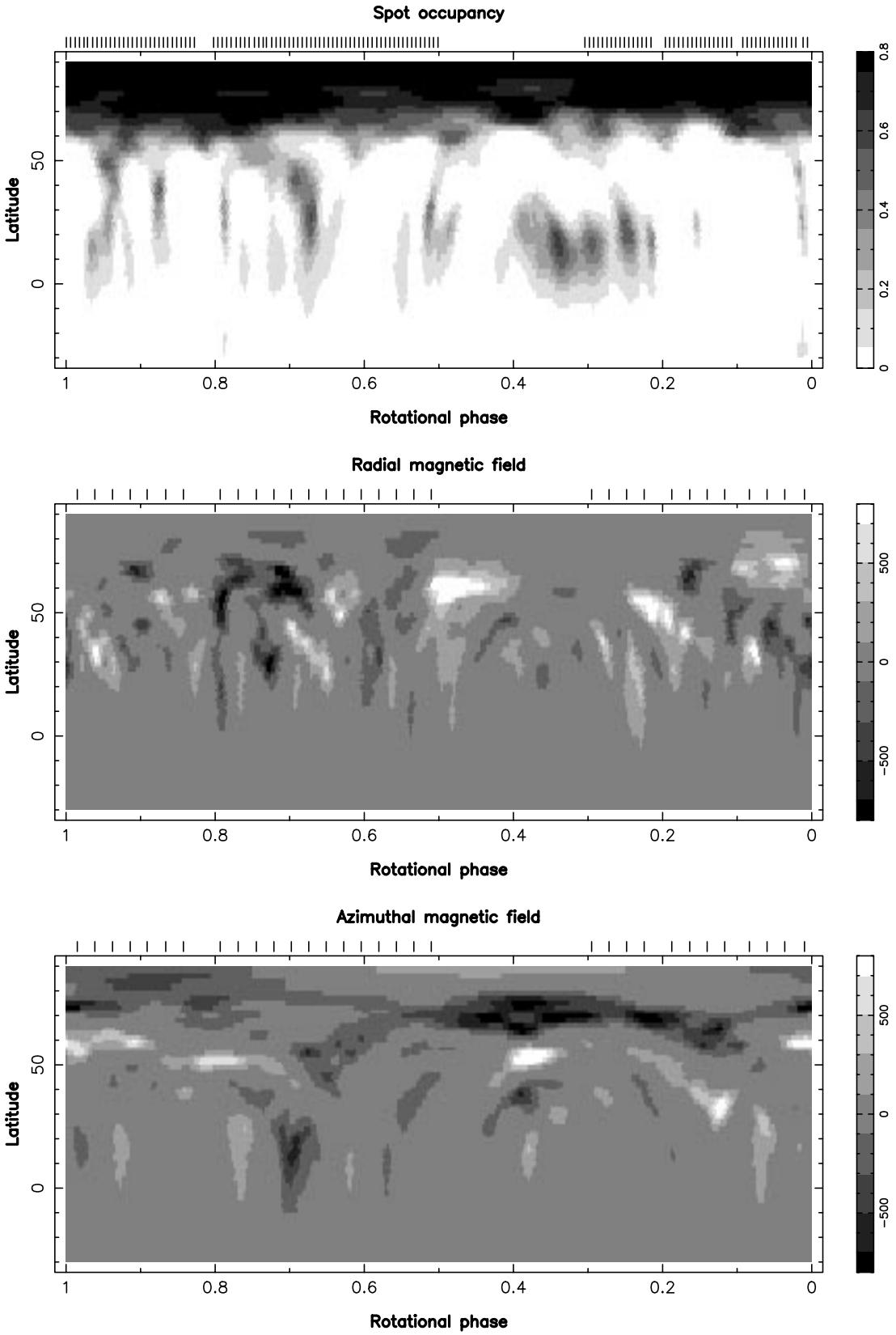

Figure 4. Maximum entropy brightness (upper row) and magnetic (lower rows) rectangular maps of AB Dor on 1996 December 23 to 25. The reconstructed meridional field component is very small and is therefore not shown here. The vertical ticks above each graph depict the rotational phases of individual Stokes *I* and *V* observations. Positive field values correspond to magnetic vectors directed outward and eastward for radial and azimuthal field components respectively (all labelled in G). The corresponding phase coverage being quite dense, the location of most surface features in these maps should be very reliable. Note that rotational phase runs backwards (i.e. from right to left) on all maps.

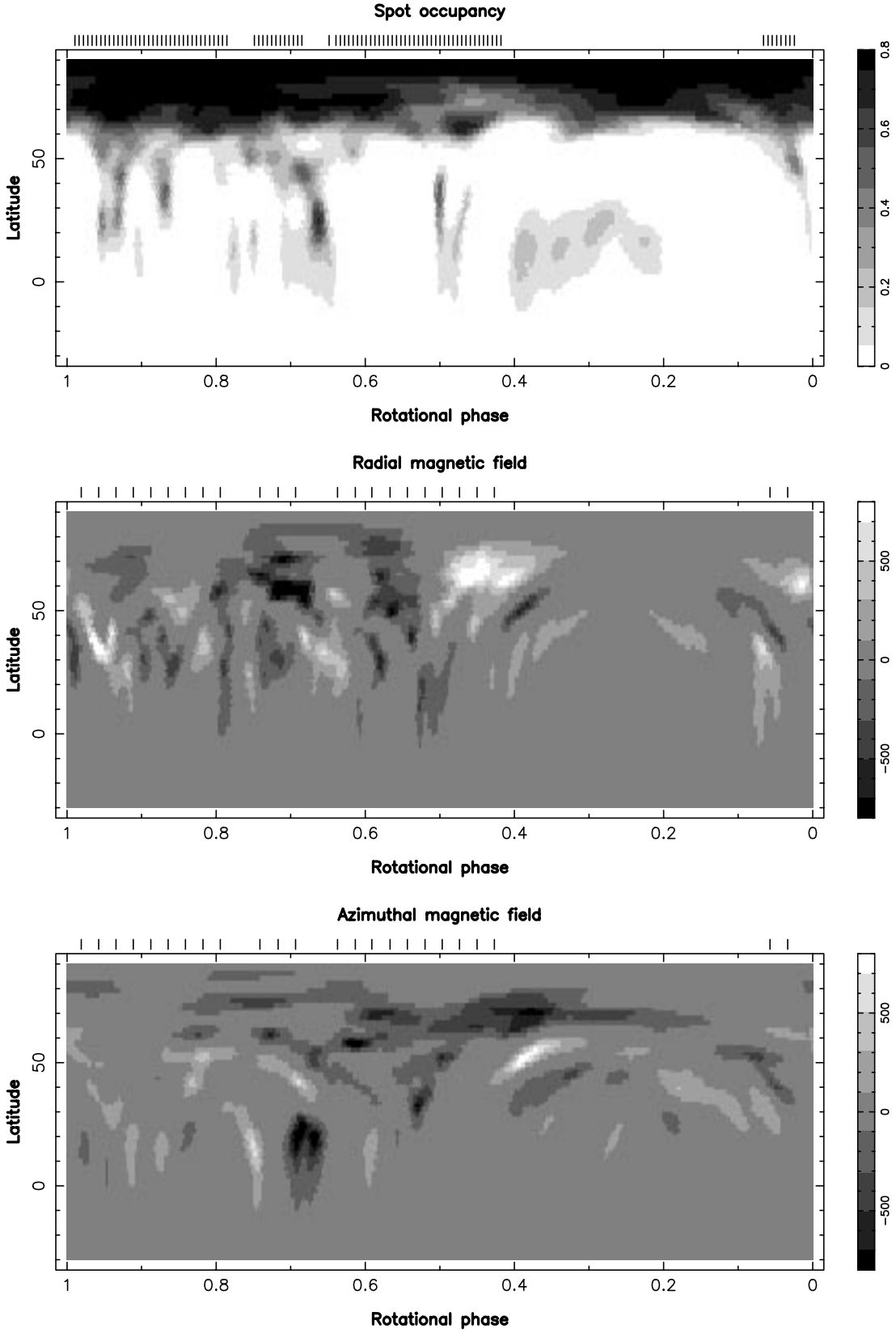

Figure 5. Same as Fig. 4 but for 1996 December 27. The big gap in phase coverage between phase 0.06 and 0.42 is responsible for the important latitudinal blurring (or non-reconstruction) of all image features located within the corresponding phase range.

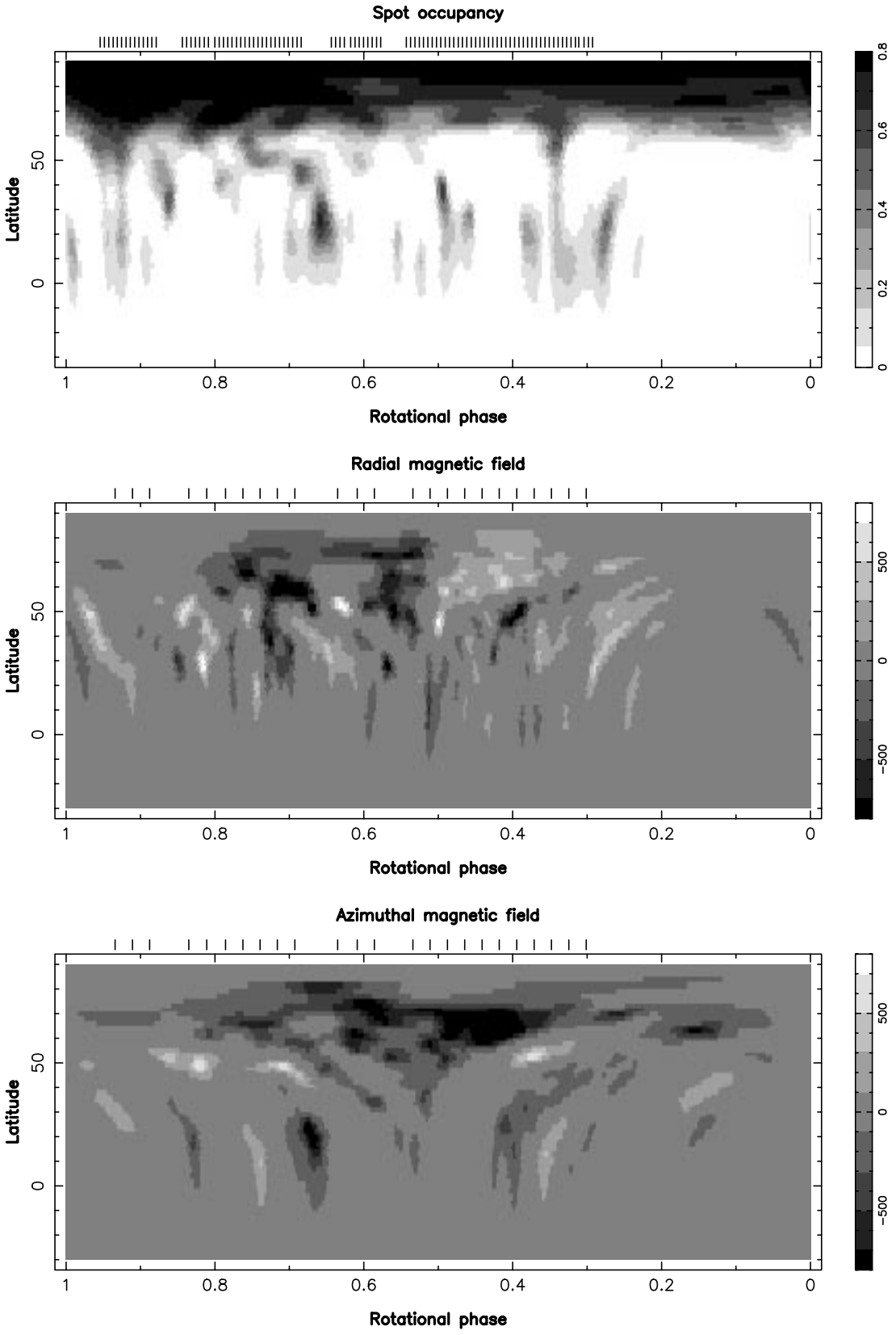

Figure 6. Same as Fig. 4 but for 1996 December 29. The big gap in phase coverage between phase −0.05 (i.e. 0.95) and 0.30 is responsible for the important latitudinal blurring (or non-reconstruction) of all image features located within the corresponding phase range.

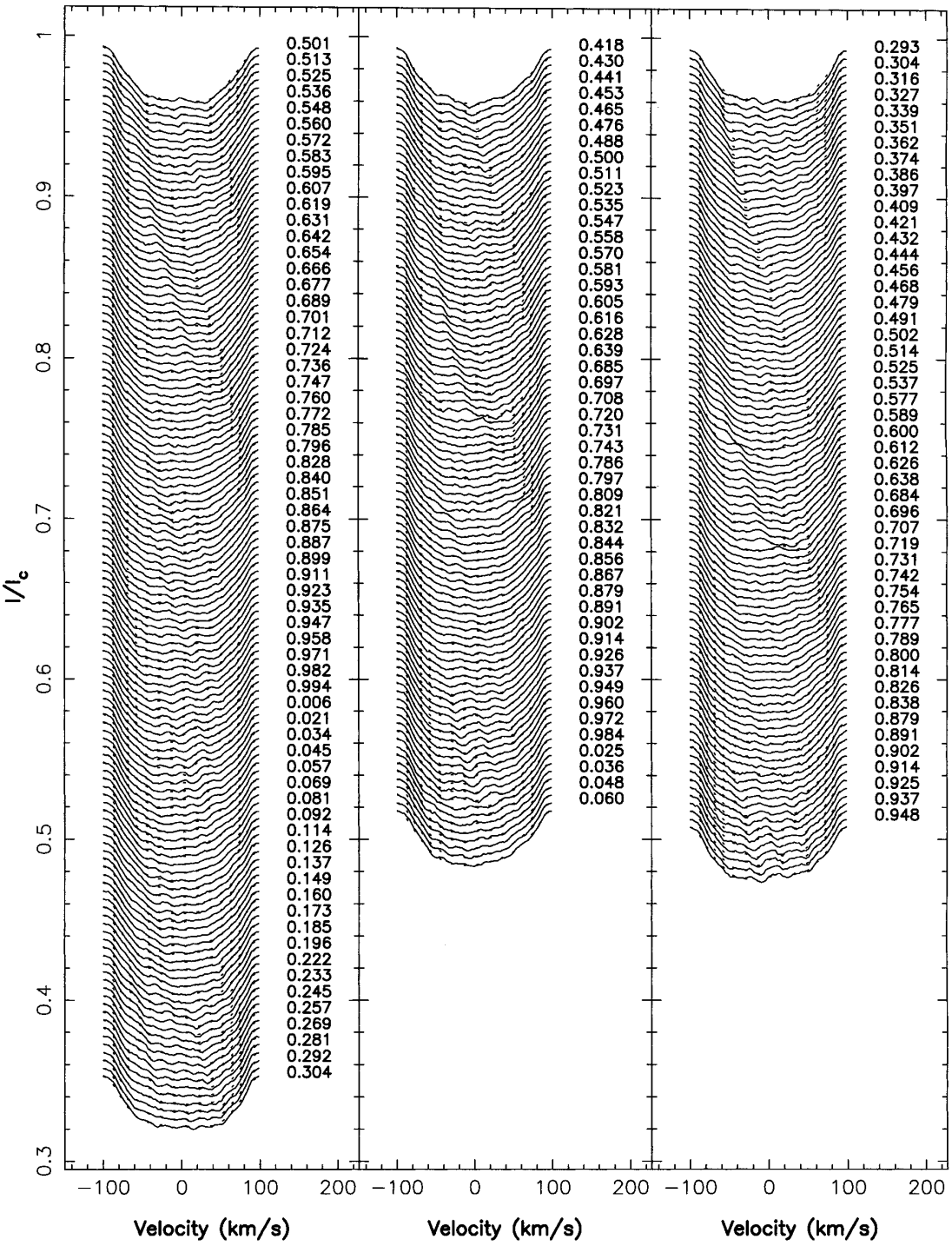

Figure 7. Observed mean Stokes *I* profiles (solid line) of AB Dor and maximum entropy fit (dotted line) for 1996 December 23, 25 (left column), 27 (middle column) and 29 (right column) data sets. Successive profiles are shifted downwards for graphics purposes. Rotational phases are noted right to each second profile.

Both radial and azimuthal field regions are observed on AB Dor in 1996 December. The radial field component features at least 12 (and possibly up to 16) different regions of opposite polarities, more or less regularly spaced in longitude. Although the agreement between the different images is not perfect in the first half rotation cycle (i.e. phase 0.0 to 0.5) owing to large gaps in phase coverage for at least one data set, it is much better for the second half cycle where most spots are detected in all three maps. Three major radial field regions (of positive, negative and negative polarity respectively) can be identified at latitude 60° (at phase 0.45, 0.55 and 0.75 respectively), with typical magnetic fluxes in excess of 1 kG. While the first one is essentially monolithic, the second and third each include as much as two individual subcomponents (at phase 0.70 and 0.80 for the third one, and latitude 50° and 70° for the second one) along with several low-latitude appendages (at phase 0.78, 0.73, 0.60 and 0.52). Clear intrinsic variability is observed for this second major radial field region, which evolved from rather weak in image #1 to relatively strong in image #3. Simultaneously,

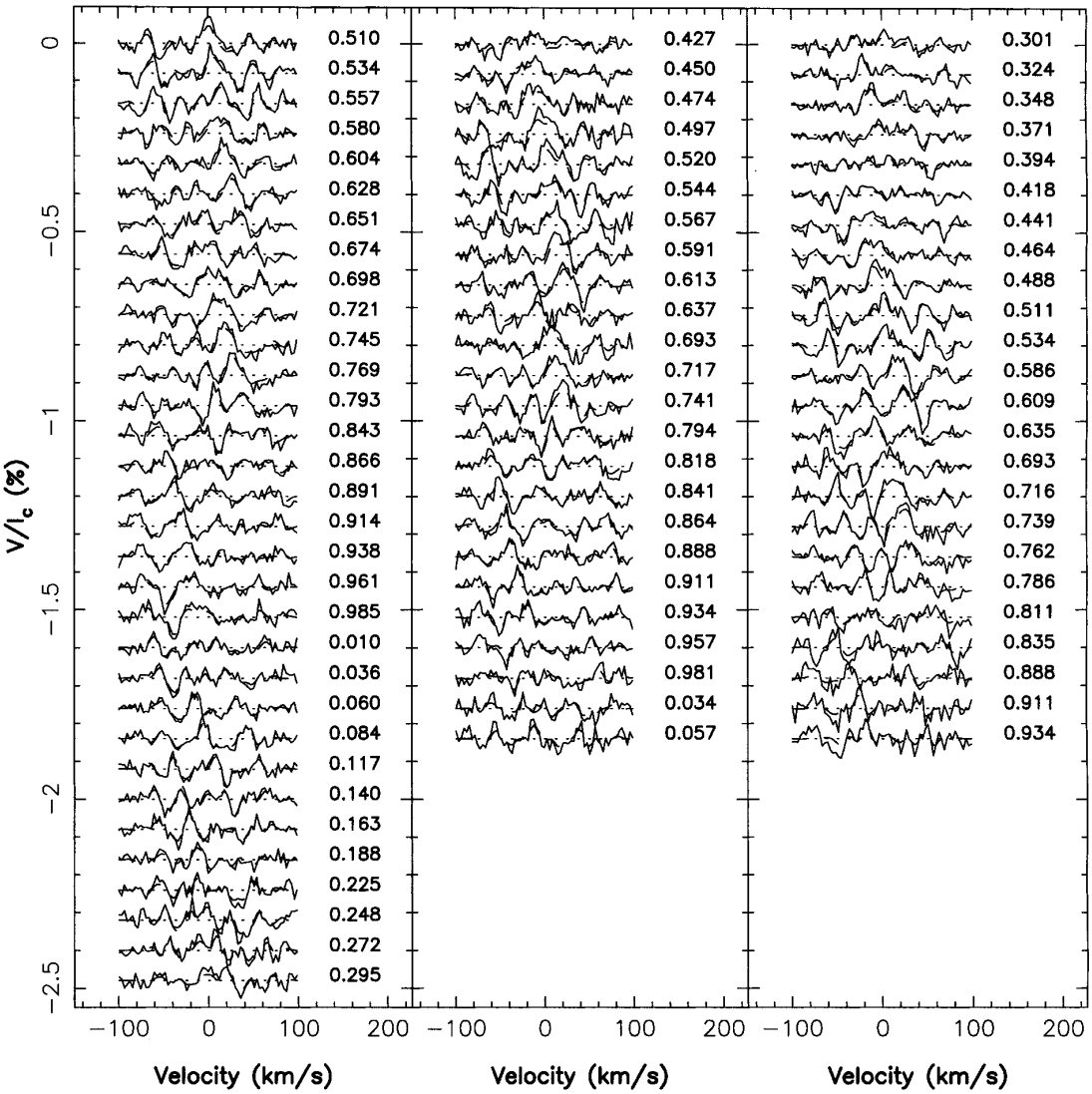

Figure 8. Same as Fig. 7 for Stokes *V* profiles. Note that the maximum entropy fit is now depicted with a dashed line while the dotted line illustrates the zero polarization level of each profile, and that rotational phases are now indicated right to each profile.

the western low-latitude appendage of the third major radial field spot (located at phase 0.78) weakened considerably within our time sequence, just as its brightness counterpart did (see previous paragraph). Note as well that most radial field features concentrate in mid to high (i.e. $> 30°$) latitudes and seem to avoid equatorial regions (i.e. below 30°), where nothing more than meridional blurring artifacts of higher latitude features are observed.

The azimuthal component of the vector field is significant, with fluxes exceeding 1 kG in several regions of the photosphere. Particularly obvious is the inhomogeneous negative polarity belt of azimuthal field encircling the rotational pole at a typical latitude of 70° to 80°, which repeats quite well in all three images. The opposite (i.e. positive) polarity dominates intermediate (i.e. 30° to 60°) latitudes, with up to five individual regions (at phase 0.00, 0.13, 0.37, 0.70 and 0.82) in which the field reaches up to 1 kG. Finally, one region of strong negative azimuthal field (located close to the equator at phase 0.68) is detected at all epochs.

No significant meridional field is observed on AB Dor. This is indeed expected for low-latitude meridional field regions to which ZDI is very weakly sensitive at high stellar inclinations (Donati & Brown 1997). However, for intermediate-to high-latitude regions, this non-detection must be considered as reliable.

3.3 Prominences

Short time-scale variations observed in the Balmer spectral lines of AB Dor are thought to be caused by the presence of prominence formations in the co-rotating frame of the star (see Cameron & Robinson 1989a,b). As these clouds cross the stellar disc, they produce absorption features in the Hα rotation profile of the star. The rate at which these absorption transients drift across the Hα profile indicates the distance of the cloud from the stellar rotation axis. If the magnetic field confining these structures is rigid, the rotation period of the cloud should indicate the rotation rate at the latitude of the loop footpoints.

We used a modified version of Cameron & Robinson's (1989a, b) back-projection techniques to measure the longitude and distances of these prominences from the stellar rotation axis for spectra taken at the AAT in December 1996, in a very similar way as we did for our 1995 December data (Donati & Cameron 1997). As the

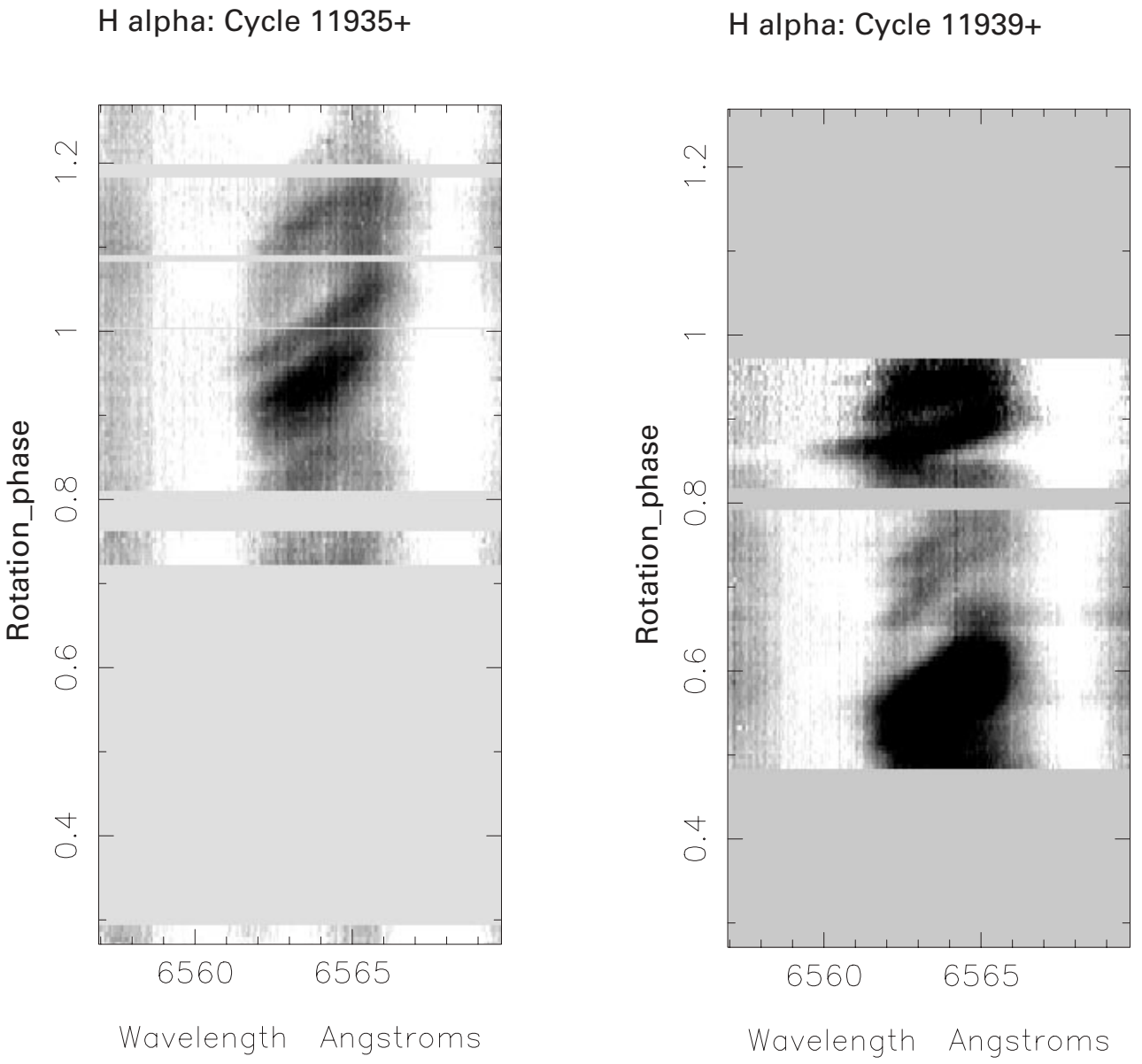

Figure 9. Dynamic spectra of the Hα profile of AB Dor for data sets from December 23 and 25 respectively. Grey levels code relative intensities (normalized to the continuum level) ranging from 0.75 (black) and 0.9 (white).

dynamic Hα spectra clearly show, (Figs 9 and 10), several cloud complexes were present around AB Dor during this period. As described previously in Donati & Cameron (1997), all spectra were unsharp-masked prior to back-projecting them, in order to maximize the contribution of sharp absorption cores in these line profiles. The process of unsharp-masking involves producing a version of the original dynamic spectra which has been Gaussian-smoothed in the wavelength direction. This smoothed image is then subtracted from the original dynamic spectra. Figs 11 and 12 show back-projected maps obtained with this procedure, which give an indication of the flux deficit owing to cloud absorption as a function of rotation phase and distance ϖ from the stellar rotation axis.

The distance of each cloud from the stellar rotation axis is estimated, at each observing epoch, by taking the value of ϖ at which the absorption trough in the back-projected map is strongest. A slice through the back-projected image at this distance is then achieved to evaluate (using a line-bisector type analysis) the time of meridian crossing for the selected prominence and observing epoch. We obtain that prominences lie some 2.5 to 4.7 $R_\star$ away from the stellar rotation axis, i.e. significantly further out than those measured in 1995 (Donati & Cameron 1997). The position of each cloud complex derived from our observations with this technique is listed in Table 2. The uncertainty on the axial distance at which a cloud is measured (typically 0.2 $R_\star$) translates into an error bar of about 0.002 per cent on the phase at which this cloud crosses the meridian.

Looking at Figs 11 and 12 in detail, we find that Aa, Ab, G and I are features that have been recovered more than once. Fig. 13 (picturing a slice at a distance of 4 $R_\star$ from the rotation axis, appropriate for features Ab, G and I, see Table 2) illustrates the phase delays between cloud complexes from night to night. Note that feature L is very likely different from feature Ab, even though they happen to be located at almost the same rotational phase; a

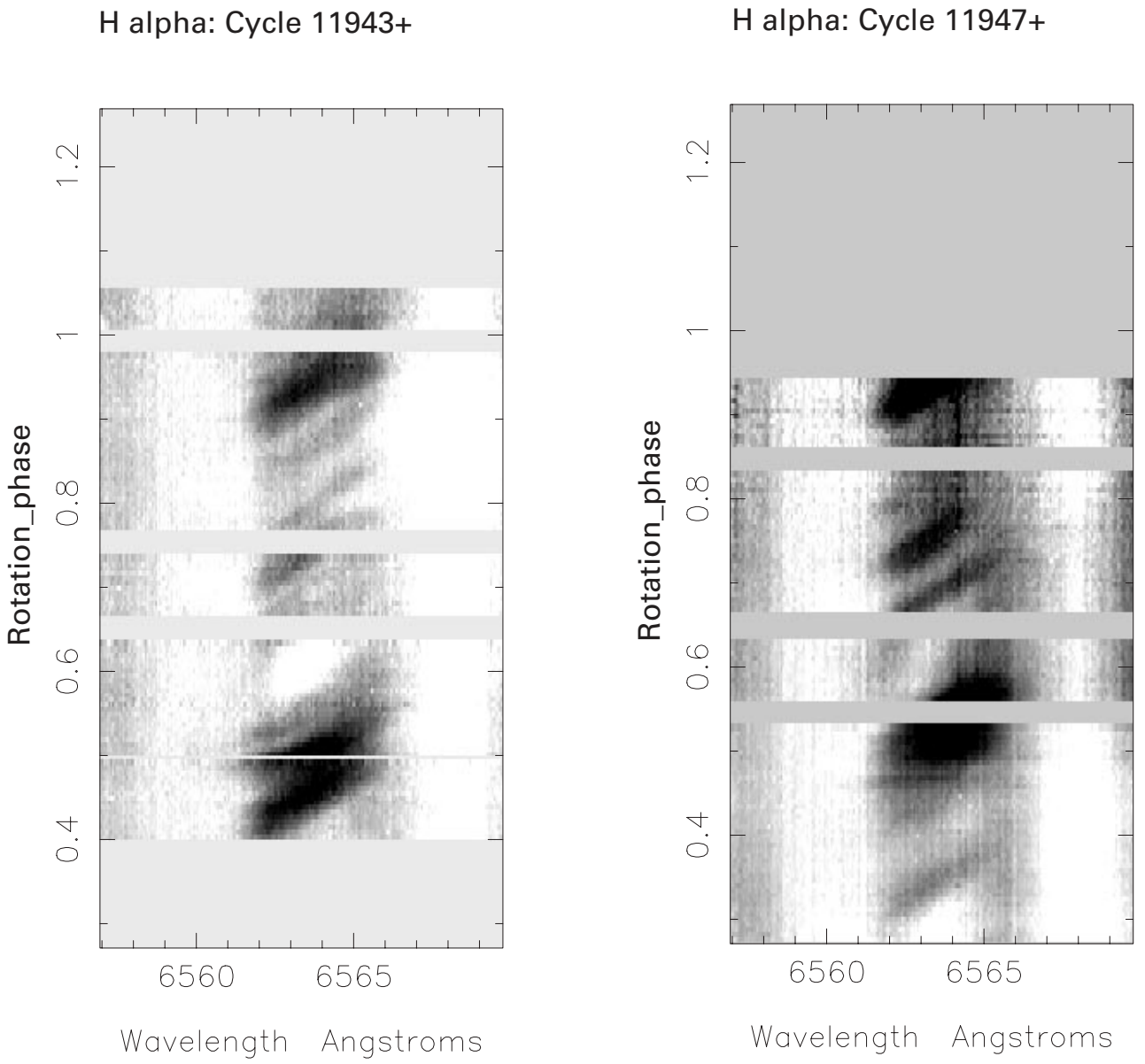

Figure 10. Same as Fig. 9 for data sets from December 27 and 29 respectively.

closer look to Figs 11 and 12 and to Table 2 reveals that the distance of feature L from the rotation axis is quite different from that of feature Ab, implying that L is probably a newly formed cloud, while Ab must have been ejected between December 25 and 27.

For the four prominences that have been measured more than once (namely Aa, Ab, G and I), we derive rotation periods of 0.5147, 0.5143, 0.5140 and 0.5156 d respectively. The error bar on the phase of meridian crossing yields a typical error bar of 0.0004 d for these estimates. All other features are shorter lived, with lifetimes of under four rotation cycles. Note that a particularly short-lived and blueshifted feature (reaching velocities of up to -180 km s^{-1}) is observed in conjunction with prominence *G* at 11939.87 (see Fig. 9, right panel), quite similar to what Cameron & Robinson (1989b) detect in their own data set. This feature is only visible for about four consecutive subexposures, i.e. about 2.4 per cent in rotational phase or 18 min.

We also detect flares on three out of the four observing nights, at cycle 11 936.24, 11 943.61 and 11 947.29. The flare measured at phase 0.61 on 27 December is still visible (though much weaker) on 29 December (see Fig. 10), indicating that it lasted over four rotation cycles.

4 DISCUSSION

4.1 Surface differential rotation

By cross-correlating constant latitude slices extracted from both brightness and magnetic maps (at phases where data set #1 and #3 overlap, i.e. from 0.50 to 0.95), we can get a precise idea of the extent to which the photosphere of AB Dor became sheared on a time-scale of eight rotations (i.e. about 4 d). The cross-correlation images are displayed on Fig. 14 and illustrate that our new data sets fully confirm the surface differential rotation curve obtained by Donati & Cameron (1997). The absence in 1996 December of truly equatorial brightness features on AB Dor in the phase range used for cross-correlation (see Section 3.2) is responsible for the broadened

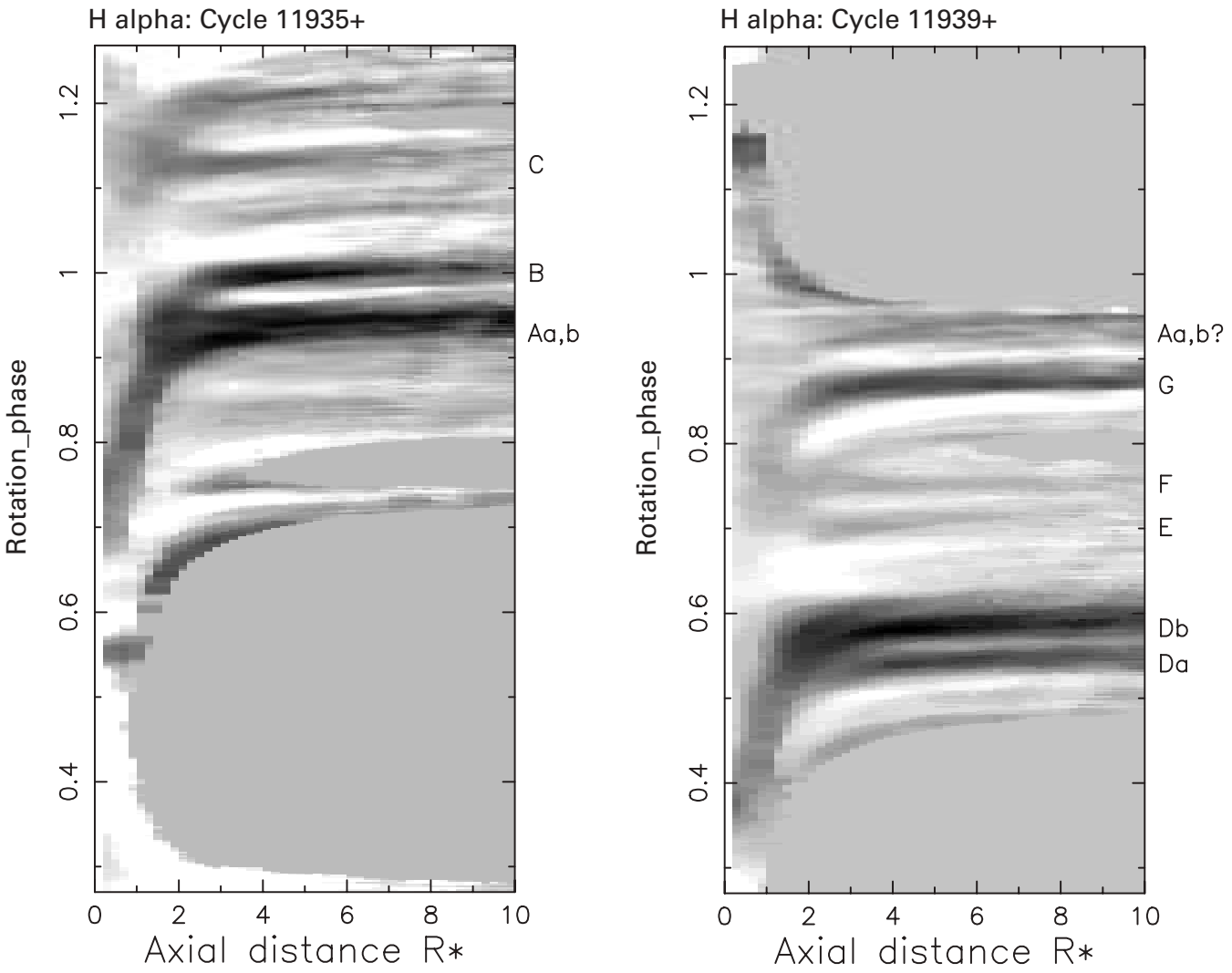

Figure 11. Back-projected maps of the Hα prominence absorption features for data sets from 1996 December 23 and 25 respectively. Each cloud listed in Table 2 is labelled on the right hand side of each graph.

cross-correlation peak below a latitude of about 20°. However, thanks to the equatorial spot of azimuthally oriented field at phase 0.68, we can confirm the surface differential rotation estimate of Donati & Cameron (1997) even at low latitudes (see lower panel of Fig. 14). Note that this result is only very weakly sensitive to the surface differential rotation law we assumed when reconstructing the maps of Fig. 4, since the phase interval on which cross-correlation is performed contains mostly brightness/magnetic features that are unaffected by this assumption (see Section 3.2).

It is interesting to note that the new brightness distribution we derived for AB Dor in 1996 December is somewhat similar to that of Donati & Cameron (1997) obtained one year before, with one major low-latitude feature around phase 0.70, and weaker ones at phase 0.55, 0.80 and 0.95. Of course, a detailed look quickly reveals that these two distributions are actually far from similar; correlating them together yields for instance a very noisy image (see Fig. 15), demonstrating that both maps have not much in common. It confirms in particular that the typical time-scale on which brightness distributions remain coherent is much smaller than one year, in agreement with the amount of surface differential rotation measured for AB Dor. A very recent study on ultra-fast rotating ZAMS cluster stars similar to AB Dor (Barnes et al. 1998) confirmed this point and demonstrated that coherence time-scale for brightness distributions are actually shorter than one month, implying that most studies measuring surface differential rotation on images shifted by one month (e.g. Vogt & Hatzes 1991; Vogt et al. 1998), one year (e.g. Hatzes & Vogt 1992; Weber & Strassmeier 1998) or even five years (Hatzes 1998) must be taken with extreme caution.

It also emphasizes that very high spatial resolution images are definitely required when comparing several images together in order to estimate surface differential rotation or spot lifetimes for instance; with low spatial resolution images, nothing more than an overall similarity between brightness distributions can be checked for (see for instance Cameron 1995), which is obviously insufficient and even potentially misleading as pointed out above.

Comparing image #1 (see Fig. 4) and #3 (see Fig. 6) around rotational phase 0.30 also illustrates how much reconstructed features can be distorted when only partial coverage is available. It is indeed quite obvious from Figs 4 and 6 that the average longitude of the multiple low-latitude spot group located at phase 0.30 is not the same in both images (not to speak about the actual

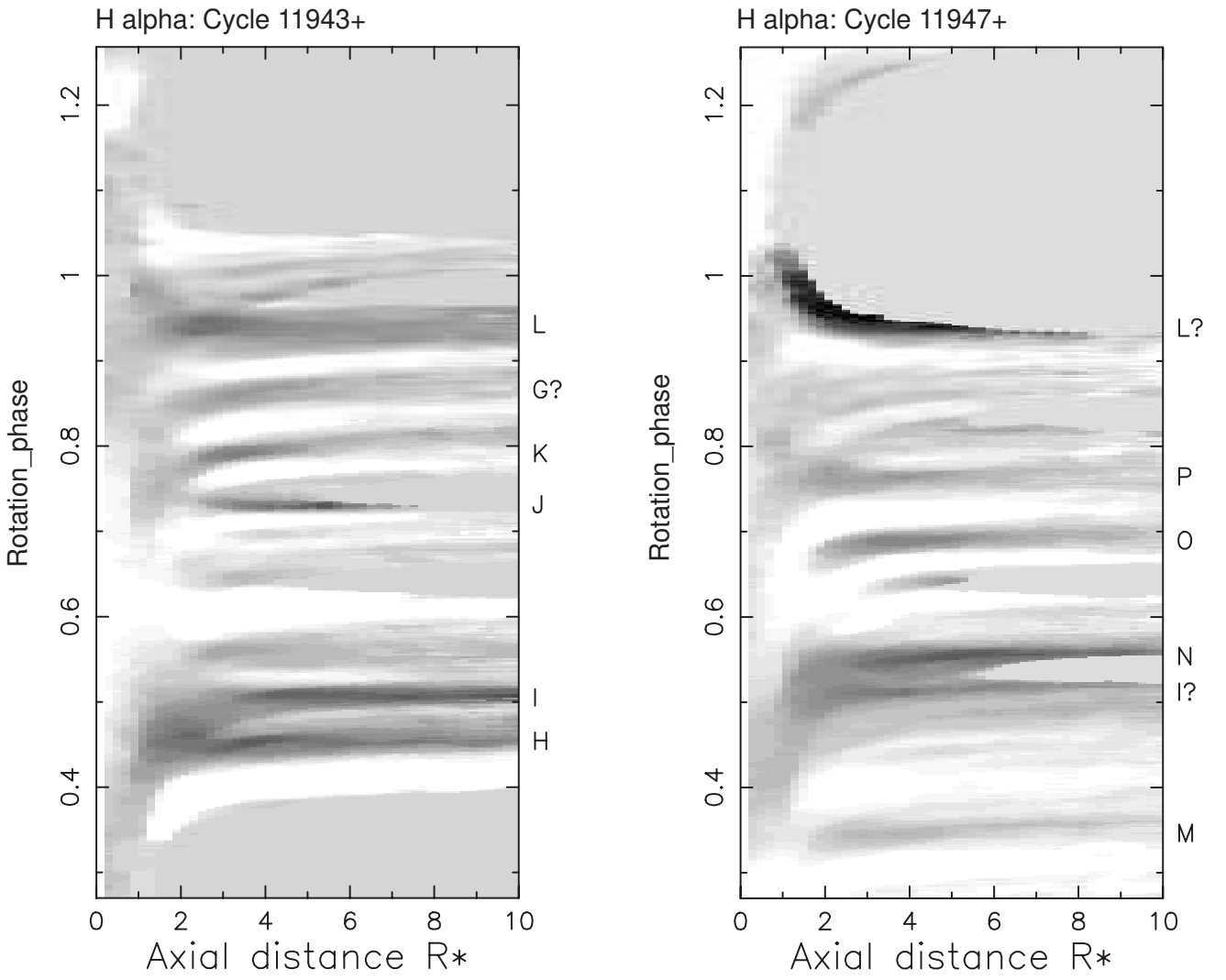

Figure 12. Same as Fig. 11 for data sets from December 27 and 29 respectively.

details of the individual subcomponents), with an apparent phase shift opposite to what would be expected given the measured surface differential rotation. In particular, this point demonstrates how crucial truly continuous coverage of the rotation cycle is when one aims at extracting subtle differential information about stellar surface features. It also implies that surface differential rotation will probably be extremely difficult to measure on cool stars with rotation periods of about a few days, for which the requisite continuous phase coverage can only be obtained with the help of multisite spectroscopic networks. Existing estimates for such stars, obtained from sparsely time-sampled images and reconstructed from data sets with non-continuous phase coverage (e.g. Hatzes & Vogt 1992; Vogt et al. 1998) must therefore also be regarded as highly uncertain.

4.2 Magnetic field topology and dynamo processes

The first important result to mention is that the polarities of the azimuthal field regions we detect on AB Dor are perfectly consistent with those derived a year before, i.e. negative at latitudes higher than 60° and positive at intermediate latitudes (30° to 60°). The higher quality data obtained this time even allowed us to demonstrate that almost a full ring of negative azimuthal field encircles the stellar rotational pole (see Fig. 4), very similar to what is found on HR 1099, another very active though much more evolved object (Donati et al. 1992; Donati 1999). In particular, it confirms the suggestion of Donati & Cameron (1997) that the azimuthal field we detect on AB Dor is indeed directly related to the toroidal component of the dynamo-generated large-scale magnetic field itself (the polarity of which is modulated on an activity cycle period time-scale, i.e. typically one decade) rather than attributable to a random manifestation of magnetoconvection within the stellar photosphere at the time of our observations.

While all magnetic regions detected by Donati & Cameron (1997) were located above a latitude of about 30°, we clearly detect in the new images a low-latitude feature of negative azimuthal field. It strongly suggests in particular that the underlying toroidal field structure undergoes at least two polarity switches in the upper hemisphere of AB Dor. Equivalently, it implies that the large-scale poloidal structure giving rise to the azimuthal field tori through the interaction with differential rotation is even more complex than an octupole (as suggested by Donati & Cameron 1997), and must therefore involve a dominant axisymmetric spherical harmonic component of (supposedly odd) degree $\ell \geq 5$. Note

Table 2. Identification and location of Hα-absorbing clouds.

Ident	Phase	$\varpi/R_\star$	Period / d
Aa	11935.924 ± 0.002	3.0 ± 0.2	
Ab	11935.941 ± 0.002	4.5 ± 0.2	
B	11936.001 ± 0.002	4.7 ± 0.2	
C	11936.129 ± 0.002	3.2 ± 0.2	
Da	11939.541 ± 0.002	4.2 ± 0.2	
Db	11939.583 ± 0.002	4.2 ± 0.2	
E	11939.702 ± 0.002	3.1 ± 0.3	
F	11939.753 ± 0.002	3.4 ± 0.2	
G	11939.870 ± 0.002	3.5 ± 0.2	
Aa?	11939.923 ± 0.002	2.7 ± 0.2	0.5147 ± 0.0004
Ab?	11939.937 ± 0.002	4.5 ± 0.2	0.5143 ± 0.0004
H	11943.454 ± 0.002	3.7 ± 0.2	
I	11943.505 ± 0.002	4.5 ± 0.2	
J	11943.732 ± 0.002	4.5 + 0.8	
K	11943.792 ± 0.002	3.2 ± 0.2	
G?	11943.867 ± 0.002	3.8 ± 0.2	0.5140 ± 0.0004
L	11943.944 ± 0.002	2.5 ± 0.2	
M	11947.346 ± 0.002	2.8 ± 0.2	
I?	11947.512 ± 0.002	3.8 ± 0.2	0.5156 ± 0.0004
N	11947.554 ± 0.002	4.5 ± 0.2	
O	11947.690 ± 0.002	3.5 ± 0.2	
P	11947.765 ± 0.002	3.8 ± 0.2	
L?	11947.94 ± 0.01		

that the presence of such high ℓ magnetic structures in rapidly rotating stars has been predicted by Schatzmann (1991). It is also worth mentioning that this large-scale field structure is apparently slightly tilted (by about 10° and towards phase 0.30) with respect to the rotation axis, both in 1995 December (see Fig. 9 in Donati & Cameron 1997) and 1996 December (see Fig. 4). Similar tilts of the magnetic structure have also been observed in other rapidly rotating late-type stars (Donati 1999).

Most numerical simulations to date agree on the fact that the common action of buoyancy and Coriolis forces in rapidly rotating cool stars should force magnetic flux tubes (from an initial supposedly solar-like toroidal field structure confined at the base of the convective zone) to emerge radially at high latitudes (Schüssler et al. 1996; DeLuca, Fan & Saar 1997). In the particular case of AB Dor whose rotation rate and convective zone depth are about 50 times solar and 0.4 $R_\star$ respectively, they find that most flux tubes should break the photosphere at a latitude larger than 35° typically. With significant azimuthal field detected at photospheric level and at low latitudes, our magnetic images of AB Dor confirm that this object must feature a significant non-solar dynamo component distributed throughout the whole convective zone. It therefore suggests that the radial rotational shear inside the convection zone itself must be significantly larger than on the Sun (for which no definite evidence of a distributed dynamo has been reported to date).

As already pointed out by Donati & Cameron (1997), the apparent spatial correlation between brightness and magnetic features is rather weak; brightness features seem for instance to avoid the major negative radial field feature at phase 0.70 and latitude 60°. However, a closer look reveals that cool spots tend to be at least statistically more magnetic than the quiet photosphere; once all image pixels are divided into 10 equally wide classes of increasing spot occupancy, we observe that the recovered mean field strength (averaged on all pixels of each class) is multiplied by a factor of three to six (depending on whether these mean field values are compensated from class-to-class brightness differences or not) when going from quiet photosphere to cool regions with 60 per cent spot occupancy (see Fig. 16). This is very similar to what was pointed out already by Donati & Cameron (1997).

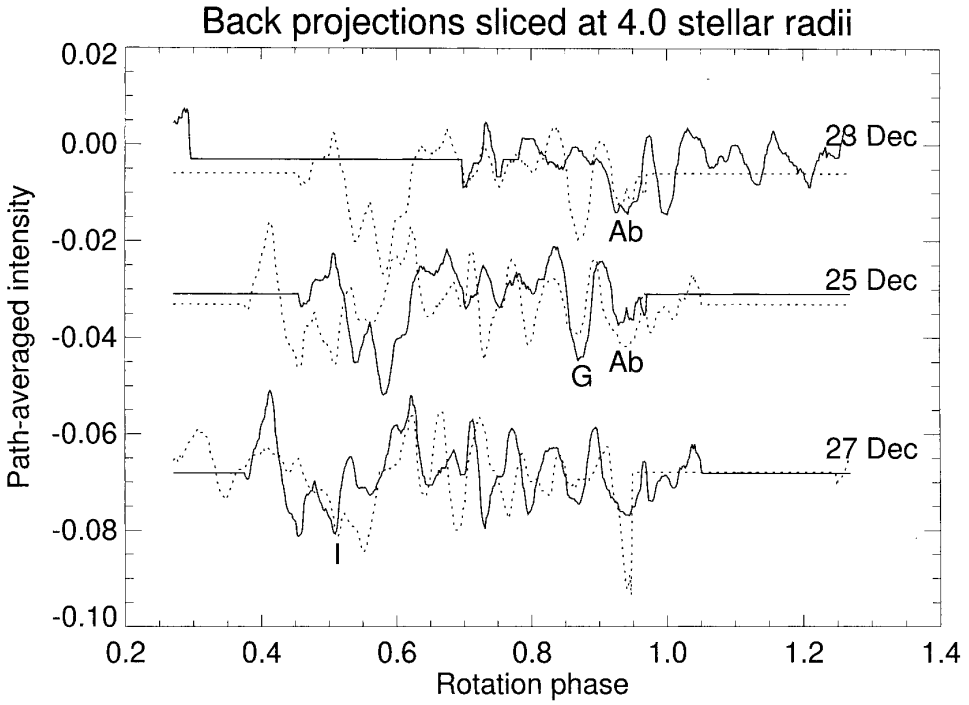

Figure 13. Slices through the back-projected maps of data sets for all 4 nights at a distance of 4 $R_\star$, showing the phase delays for prominences Ab, G, I (located at a distance of about 4 $R_\star$). For each of the first three nights, the solid line depicts the current slice (labelled with the appropriate date) while the dotted line indicate that of the subsequent observing night.

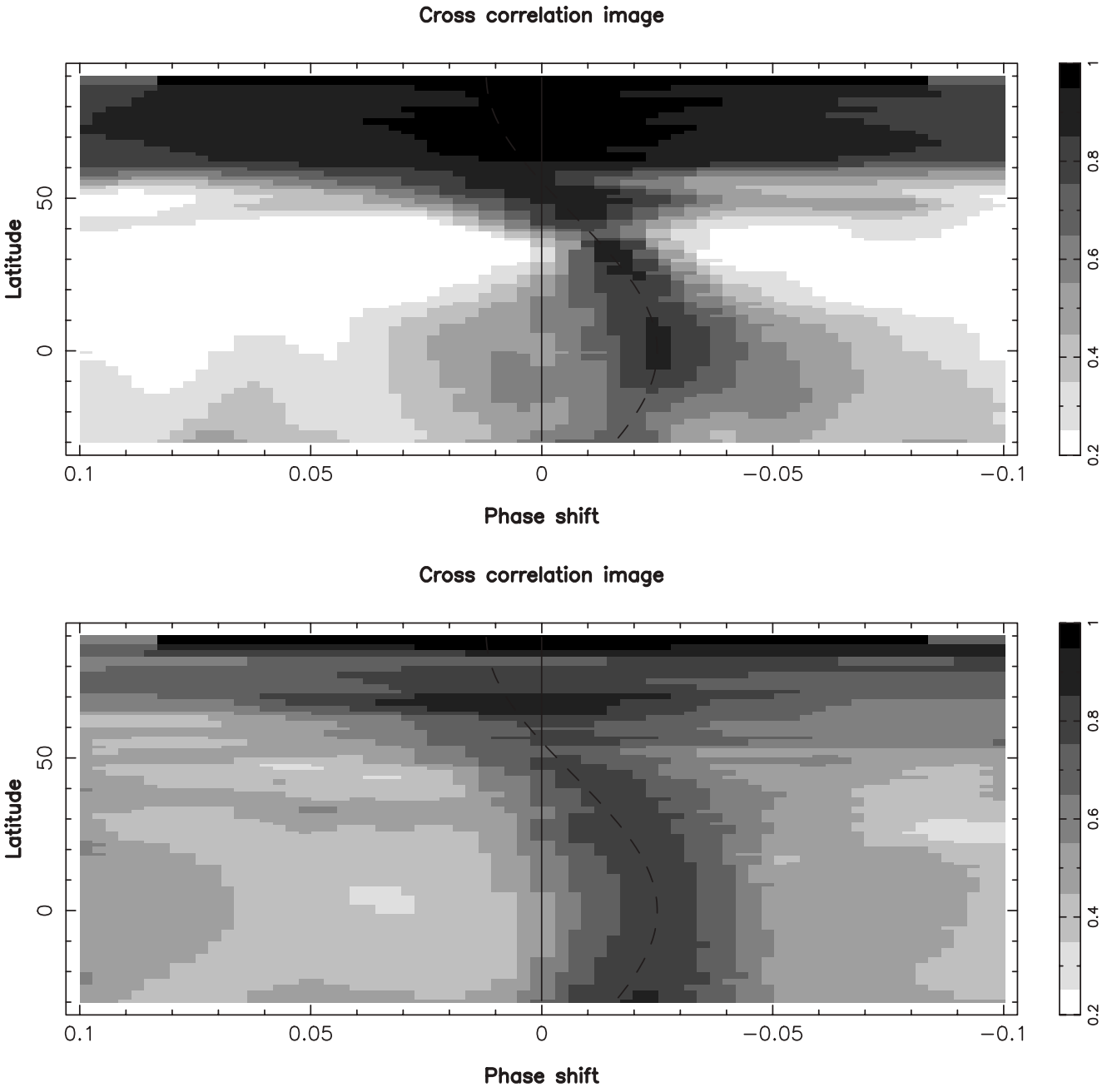

Figure 14. Cross-correlation images obtained by cross-correlating each latitude belt of image #1 (see Fig. 4) and image #3 (see Fig. 6) on phase interval [0.50,0.95], for brightness (upper panel) and magnetic field (lower panel). The magnetic cross-correlation image is the geometrical mean of both radial field and azimuthal field cross-correlation maps. The dashed line in each panel depicts the surface differential rotation curve derived by Donati & Cameron (1997). Note that negative phase shifts imply faster rotation, while the opposite (less natural) convention was used in Donati & Cameron (1997).

4.3 Prominences

We detected about 16 prominence complexes around AB Dor in 1996 December, most of them being structures with lifetimes shorter than four rotation cycles. The majority of these prominences appear to lie at a distance of about 4 $R_\star$, i.e. significantly further out than those measured in 1995 December (Donati & Cameron 1997) and than the corotation radius (equal to 2.5 $R_\star$ at the equator level). This is consistent with the fact that the clouds are less stable and thus rather shorter lived (the centrifugal force being no longer compensated by gravitation outside the corotation radius) than those studied by Donati & Cameron (1997). Among the longest lived prominences we observed (whose lifetime ranges between 4 and 8 rotation cycles, enough for us to observe them twice), we derive rotation periods that are comparable or longer than Innis et al.'s (1988) rotation period of 0.51479 d, but still within the range of period found on the stellar surface. It therefore confirms Donati & Cameron's (1997) conclusion that these structures are indeed confined by the stellar magnetic field in a state of enforced corotation. Using the surface differential rotation curve obtained by Donati & Cameron (1997), we obtain that prominences Aa, Ab, G and I (the rotation periods of which are equal to 0.5147, 0.5143, 0.5140 and 0.5156 d respectively) are anchored at latitudes 53°, 43°, 36° and 90° respectively, with an uncertainty of about 10° for

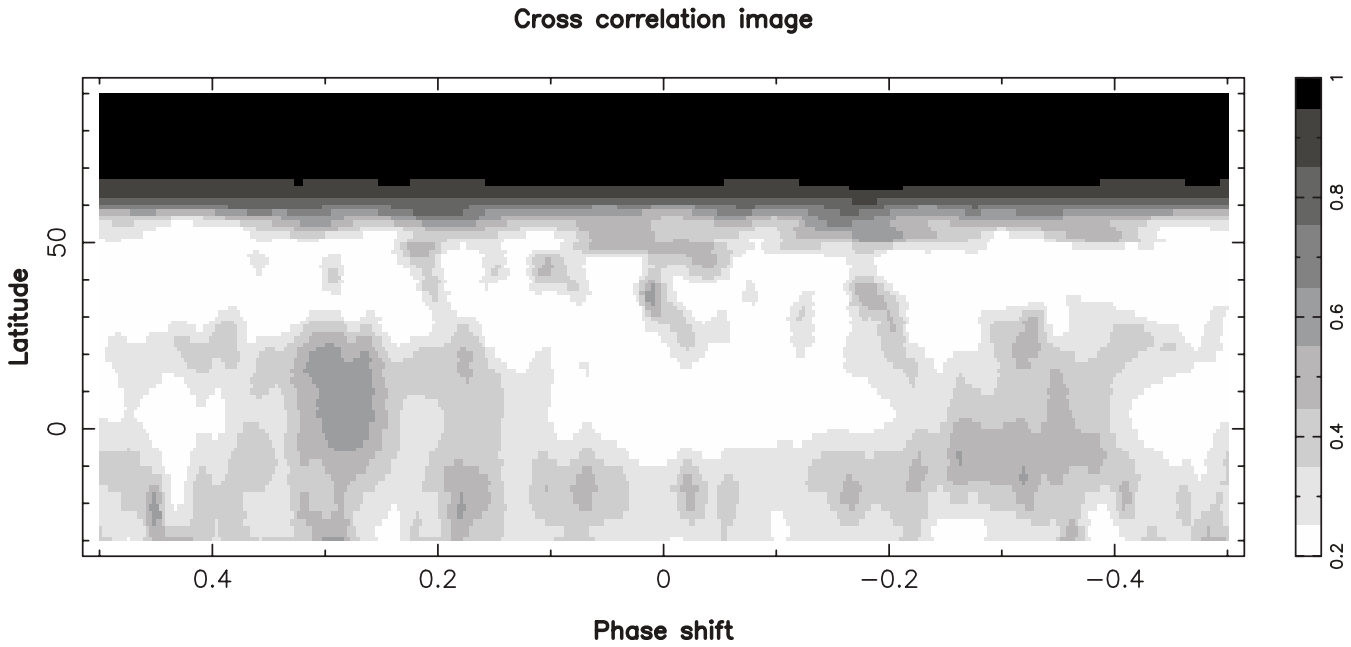

Figure 15. Cross-correlation image obtained by cross-correlating image #1 (see Fig. 4) with image #2 of Donati & Cameron (1997). Note that the scale on the phase shift axis is different than that of Fig. 14.

intermediate ones and 20° for the polar one. This is also consistent with the requirement that the prominences should be located some distance above the equatorial plane in order to transit the stellar disc (Cameron 1996).

Given the complexity of the reconstructed magnetic topology, it is not obvious to identify unambiguously which magnetic bipolar group is likely to host the footpoints of the coronal loop confining a given prominence. If it is encouraging to observe that the four prominences for which we could derive footpoint location estimates seem to gather close to the radial field polarity inversion line (see Fig. 17), one should keep in mind that this test is not altogether very conclusive given the large error bars on prominence latitudes and the intricate shape of the radial field neutral line. With denser data sets covering in particular several successive rotational cycles, one should be able in the near future to perform similar tests with enhanced precision, and hopefully conclude whether the footpoints of the prominence-bearing loops correspond to adjacent magnetic regions of opposite polarities, or to much more distant ones.

We also report the detection of high-velocity coronal plasma escaping the star at a speed of up to -180 km s^{-1}, very similar to what Cameron & Robinson (1989b) describe for another particularly short-lived feature. Being visible for no more than 18 min (see Fig. 9), this high-velocity structure can therefore not be attributed to some eruptive phenomenon occurring close to the stellar surface as it would be visible for a longer time-span. The most likely explanation is therefore that of Cameron & Robinson (1989b), i.e. that we observed a high speed cloud at a large distance from the star through its transit across the stellar disc. Note that this interpretation also explains why only very few such events are observed, the detection probability of a cloud being inversely proportional to the square of its distance from the star. Assuming this cloud is in corotation, the disc transit time of 18 min translates into a distance of at least 13 $R_\star$ away from the rotation axis. We speculate that this cloud is not a quiescent prominence (which usually drifts away five to 10 times slower with field lines being distorted in a quasi-static manner), but rather an eruptive one (even though we did not detect the associated flare) with a more energetic ejection mechanism (like coronal mass ejections following reconnecting field lines).

One point worth noting though is that none of the changes in the prominence system seem to have clearly identifiable counterparts in the photospheric maps. For instance, no apparent evolution of the magnetic image (that cannot be explained by differences in phase coverage) is observed around rotational phase 0.88 between December 23 and 27, i.e. simultaneously with the rapid cloud ejection mentioned above. It therefore strongly suggests that most of the intrinsic variability observed at coronal level is a result of local reorganization of field lines up in the corona, rather than to a rapid local evolution of the magnetic topology at photospheric level (e.g. emergence of new magnetic flux, cancelling magnetic features).

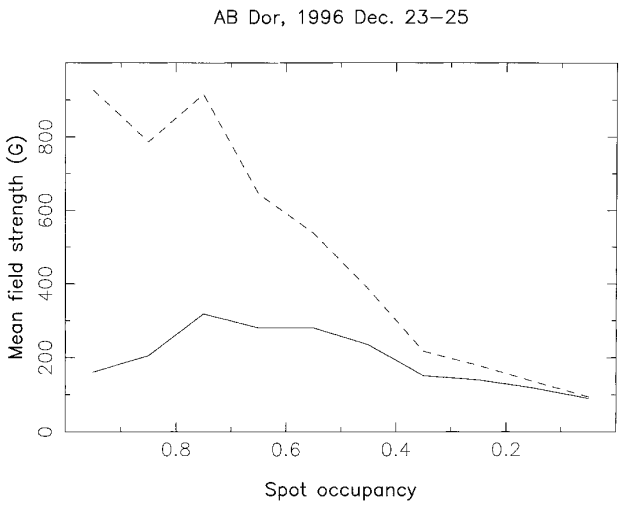

Figure 16. Mean field strength on AB Dor (1996 Dec. 23–25) as a function of spot occupancy, before (solid line) and after (dashed line) compensating for surface brightness inhomogeneities.

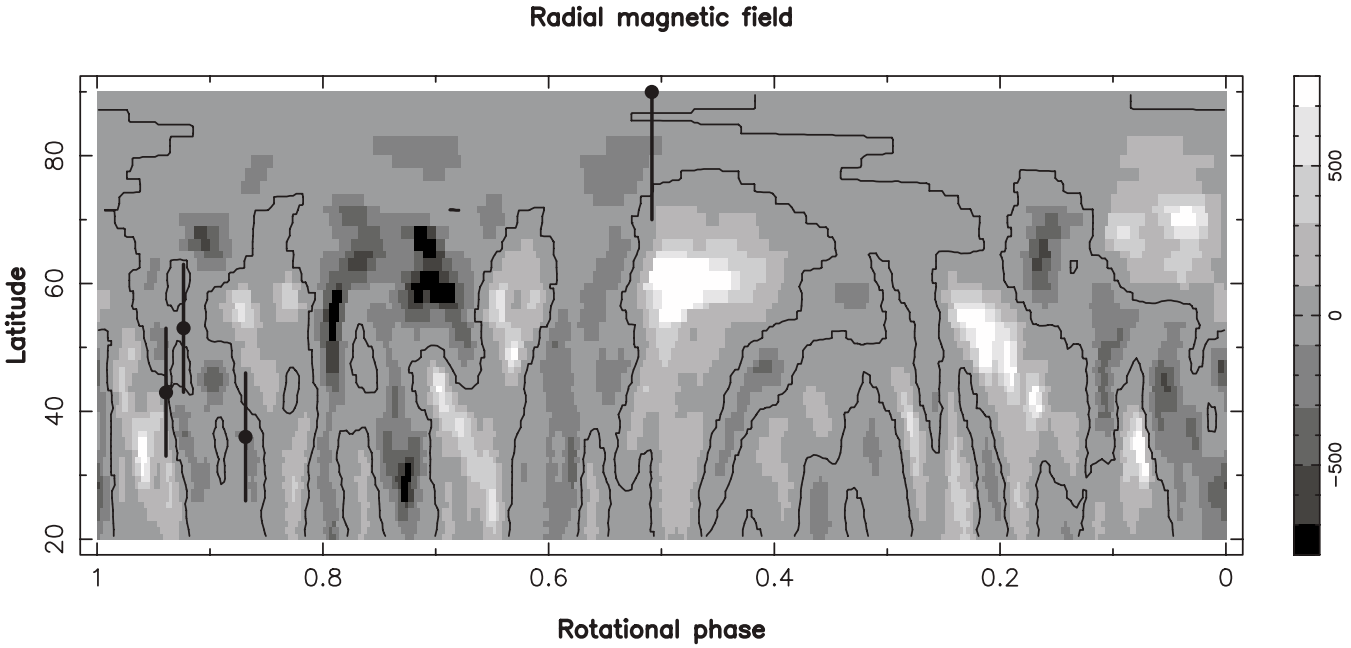

Figure 17. High-latitude close up of the radial field map from data set #1 (see Fig. 4), with contours depicting the polarity inversion lines. The four bold dots and error bars indicate the approximate footpoints location for prominence Aa, Ab, G and I as derived from their times of meridian crossing and recurrence rates (see Sections 3.3 and 4.3).

5 CONCLUSIONS AND PROSPECTS

From new spectropolarimetric data collected at the AAT, we derived simultaneous brightness and magnetic maps of AB Dor in 1996 December 23 to 25, 27 and 29. The time distortion of these distributions is perfectly compatible with the rate of surface differential rotation estimated previously from similar images by Donati & Cameron (1997).

The magnetic topology of AB Dor is found to be very complex, with at least 12 different radial field regions of opposite polarities located all around the star. Significant azimuthal field regions are also detected at photospheric level on AB Dor in the form of an almost complete negative polarity ring encircling the pole at high latitudes as well as a series of positive polarity spots at intermediate latitudes, i.e. very similar to what was observed on this star in 1995 December (Donati & Cameron 1997). In particular, it confirms our earlier presumption that such features represent a direct detection of the underlying large-scale toroidal structure of AB Dor. The almost purely azimuthal field feature of negative polarity detected close to the equator in our new data demonstrates that this toroidal structure undergoes at least two polarity switches from the equator to the pole and that the degree of the parent large-scale poloidal structure in an axisymmetric spherical harmonics expansion is equal to or greater than five. It also strengthens the idea that the dynamo processes operating in AB Dor do feature a non-solar component distributed throughout the convective zone.

Most of the 16 prominences detected around AB Dor in 1996 December have lifetimes shorter than four rotation cycles, consistent with the finding that they lie significantly outside the corotation radius. Among the longest lived prominences, four can be traced at two different epochs; the corresponding recurrence rates indicate that the associated loop footpoints are located at intermediate to high latitudes, in agreement with the predictions of Cameron (1996). The intrinsic variability of prominences does not seem to be connected with any abrupt change in the underlying photospheric field distribution and must therefore be attributed to a local reorganization of coronal field lines.

This second study of the magnetic topology of AB Dor and its relation with the coronal prominence system therefore confirms and amplifies most of the results obtained in the first one (Donati & Cameron 1997). To go ahead in the same direction, future observations should therefore concentrate on two goals. The first one is to obtain as continuous a coverage as possible for several consecutive rotation cycles, and study in much more details the distribution of prominences with respect to the underlying field topology. By extrapolating the measured photospheric field structure into the corona, we may even be able to pinpoint the footpoints of each prominence as unipolar magnetic regions in our maps. The other longer term goal consists in following the evolution of the field topology (and in particular the polarity of the large-scale toroidal component) as the star progresses on its activity cycle, and to check whether differential rotation is affected throughout the cycle as various authors speculate (Applegate 1992; Lanza, Rodonò & Rosner 1998).

ACKNOWLEDGMENTS

JFD acknowledges CNRS (UMR 5572) and AFCOP (Australia-France COoperation Programme) for travel funds and living expenses on this AAT observing run. ACC acknowledges the support of the UK Panel for Allocation of Telescope Time for the award of telescope time and for travel and subsistence funding. We thank the referee, R. Robinson, for suggesting several modifications that improved and clarified the paper. This work is based on data collected with the UCL Echelle spectrograph at the Anglo-Australian Telescope.

REFERENCES

Applegate J. H., 1992, ApJ, 385, 621

Brown S. F., Donati J. -F., Rees D. E., Semel M., 1991, A&A, 250, 463
Cameron A. C., 1992, in Byrne P. B., Mullan D. J., eds, Surface Inhomogeneities on Late-Type Stars. Springer, Berlin, p. 33
Cameron A. C., 1995, MNRAS, 275, 534
Cameron A. C., 1996, in Strassmeier K. G., Linsky J. L., eds, Proc. IAU Symp. 176, Stellar Surface Structure. Kluwer Academic Publishers, Dordrecht, p. 449
Cameron A. C., Robinson R. D., 1989a, MNRAS, 236, 57
Cameron A. C., Robinson R. D., 1989b, MNRAS, 238, 657
Cameron A. C., Unruh Y. C., 1994, MNRAS, 269, 814
DeLuca E. E., Fan Y., Saar S. H., 1997, ApJ, 481, 369
Donati J.-F., 1999, MNRAS, 302, 457 (Paper II, this issue)
Donati J.-F., Brown S. F., 1997, A&A, 326, 1135
Donati J.-F., Brown S. F., Semel M., Rees D. E., Dempsey R. C., Matthews J. M., Henry G. W., Hall D. S., 1992, A&A, 265, 682
Donati J.-F., Cameron A. C., 1997, MNRAS, 291, 1
Donati J.-F., Semel M., Carter B. D., Rees D. E., Cameron A. C., 1997, MNRAS, 291, 658
Hatzes A. P., 1998, A&A, 330, 541
Hatzes A. P., Vogt S. S., 1992, MNRAS, 258, 387
Kürster M., 1996, in Strassmeier K. G., Linsky J. L., eds, Proc. IAU Symp. 176, Stellar Surface Structure. Kluwer Academic Publishers, Dordrecht, p. 477
Kurucz R. L., 1993, CDROM # 13 (ATLAS9 atmospheric models) and # 18 (ATLAS9 and SYNTHE routines, spectral line database)
Lanza A. F., Rodonò M., Rosner R., 1998, MNRAS, 296, 893
Schatzman E., 1991, in Cox A. N., Livingston W. C., Matthews M. S., eds, Solar Interior and Atmosphere. Univ. of Arizona Press, Tucson, AZ, p. 192
Schüssler M., Caligari P., Ferriz-Mas A., Solanki S. K., Stix M., 1996, A&A, 314, 503
Skilling J., Bryan R. K., 1984, MNRAS, 211, 111
Vogt S. S., Hatzes A. P., 1991, in Tuominen I., Moss D., Rüdiger G., eds, Proc. IAU Colloq. 130, The Sun and Cool Stars: Activity, Magnetism, Dynamos. Springer, Berlin, p. 297
Vogt S. S., Hatzes A. P., Misch A. A., Kürster M., 1998, ApJS, in press
Weber M., Strassmeier K. G., 1998, A&A, 330, 1029

This paper has been typeset from a TEX/LATEX file prepared by the author.